Proc. Schl. Eng. Tokai Univ., Ser. E
40 (2015) 109-119

Airflow Patterns within Real and 3D Simplified Models of Nasal Cavities (Ⅱ. Numerical Study)

by

Erny AFIZA[*1], Yoko TAKAKURA[*2], Taku ATSUMI[*3] and Masahiro IIDA[*3]

(Received on Mar. 31, 2015 and accepted on Jul. 15, 2015)

Abstract

The human nasal cavity is comprised of complex structures with delicate geometry. Its features make it difficult to elucidate roles of the nasal morphology. In Part I (Experimental Study) of the series of this study, anatomically realistic and simplified modelling of the human nasal cavity was presented. Here as part of an extensive study, modification has been imposed on the conventional simplified models adopted in Part I to express the narrow passageway in the upper common meatus and at the vestibule of the nose in order to clarify the roles and functions in morphology of each part. Next numerical experiments have been carried out, and the relevancy of airflow patterns between realistic and modified simplified models has been discussed. As results, insights on the roles in morphology have been obtained as follows: 1) by narrowing the upper side of the cavity, the flow tends to pass along the media meatus instead of the middle and superior regions; 2) the conchae play a role as guide plates to distribute the flow more uniformly with restriction of swirl formations; 3) the role of the media concha is to determine the airflow distribution in the three meatus: the longer media concha makes the flow pass the media meatus; and 4) the nasal valve plays a role in the occurrence of recirculation in the olfactory region and also to reduce reversed flow in the inferior meatus during inspiration. Thus, complicated phenomena within the real model have been comprehended with the help of simplified models.

Keywords: Nasal cavity, Elucidation of roles, Modelling, Numerical simulation

1. Introduction

The human nasal cavity is defined as large air-filled space from the nasal vestibule to the opening of pharynx. As part of the respiratory system in the human body, it serves as the main conduit for the inspired air between external environment and human lungs. The nasal passages have aerodynamic structures lined with mucosal tissue which acts as an air-conditioner to warm and humidify the inhaled air. Besides olfactory function to aid us in sense of smell and taste, the existence of short hair at the nasal vestibule also helps preventing the harmful material from entering our lungs. During inspiration, the inhaled air enters the nostril, goes through the narrowest area in the nasal cavity, nasal valve[1)], then passes along the turbinate region before reaches the lungs where eventually the gas exchange takes place.

The nasal valve is located at the anterior region and known to have the greatest nasal airflow resistance due to the smallest cross sectional area within the nasal cavity[2)], which can cause either disturbance or assistance to the airflow during nasal respiration.

Meanwhile, nasal conchae (nasal turbinates) which consist of inferior, media and superior conchae take the wing-like structures emerging from the lateral wall covered by mucosal tissue. They play important roles in guiding and preparing the inhaled air to be alveolar condition before entering our lungs. Variation on its feature between individuals, such as length of the conchae, may affect the airflow behaviour and thus its physiology[3)].

In this field, simplification in modelling process is almost unavoidable due to the complicated features and geometry as mentioned in the previous paragraph. Although it may introduce inaccuracies in the results, in view of convenience, the advantages of the simplified models is undeniable[3, 4, 5)]. Simplified models allow variations in the geometry, such as removal and addition of features, to be implemented effortlessly. Moreover, the variations on the geometry of the cavity itself are crucial considering the features difference among individuals. Therefore, simplified models are exceptionally advantageous to understand extensively on the relationship of the airflow patterns with structural changes in the nasal cavity without consuming much time and cost.

Although, in vivo experiment is known to be most accurate as the natural nasal condition can be preserved, for example the properties of the lining tissue, however, direct physical measurements in the human nasal cavity are almost impossible due to the complexity of the geometry: crooked bends and narrowness. Thus, computational fluid dynamics (CFD) method has widely emerged between the researchers to overcome these

*1 Graduate Student, Course of Science and Technology
*2 Professor, Course of Science and Technology
*3 Assistant Professor, School of Medicine
*4 Professor, School of Medicine

experimental difficulties[6, 7]. It has been generally accepted in the study of intranasal flows that the outcomes between experimental visualization method such as Particle image velocimetry (PIV) and numerical method is approximately identical[8, 9, 10]. However, when CFD is applied to larger scale and time variable problems, the validation and verification of computational results are still required by comparison with experimental visualization, etc.

In previous work, the authors have carried out in vivo experiments to visualize the airflow patterns by the PIV method. First, pseudo two-dimensional simplified models were presented[3)11)], then three-dimensional simplified models were designed which consist of common meatus and 3D turbinates inside a pseudo 2D cavity model[12)], and the relevancy of airflow patterns was investigated between the simplified models and the real-geometric models[3)11)12)]. In Part I (Experimental Study) [13)] of series of this study, as experimentally extensive study, the airflow patterns in the above 3D models were discussed in detail. The effects of variation in nasal morphology in simplified models are investigated in attempt to clarify its morphologic roles and functions physiologically. Consequently new knowledge about the roles and functions of conchae and nasal valve were derived. However, a few discrepancies of flow patterns remain between anatomically realistic and simplified models.

Here, as extensive study succeeding to these findings[13)], numerical methods are adopted because they enable us to produce more information that is inaccessible by experimental methods such as the mass flow rate and flow patterns in detail. Furthermore, patching of nasal parts can be easily performed by use of simplified models. First, modification is shown on the conventional simplified modellings adopted in Part I[13)] to express the narrow passageway in the upper common meatus and at the vestibule of the nose. Then numerical results are shown to discuss relevancy of airflow patterns between the realistic model and the modified simplified models with variation of nasal features in attempt to clarify the morphology of nasal features.

2. Models for numerical simulation

In this study, two types of human nasal cavity models were generated: anatomically realistic model and simplified models. The details of the condition at nostril and trachea area of both models are as shown in Tables 1 and 2.

Table 1. Condition at nostril area of both models

Nostril				
Model	Area (mm^2)	Hydraulic diameter (mm)	Velocity (m/s)-	Reynolds number
Real	39.6	5.76	2.30	880
Sim-plified	40	5.71	2.31	880

Table 2. Condition at trachea area of both models

Trachea		
Model	Area (mm^2)	Velocity (m/s)-
Real	47.6	1.9
Simplified	100	0.924

2.1 *Generation of models and grids*

The anatomically realistic model was derived from a high-resolution Computed Tomographic (CT) scan of a Japanese adult. For the simplified models, the passage way in the nasal cavity was intentionally truncated, which consist of only the main parts. The airflow patterns for these two types of models are then evaluated from the simulation results and the relevancy is discussed.

2.1.1 *Anatomically Realistic Model*

By collaboration with Tokai University Hospital and Sony Corporation, a highly detailed configuration model of the human nasal cavity was fabricated as shown in Fig. 1. The three-dimensional nasal cavity model was reconstructed from a CT scan with spatial resolution 512x512 pixels, obtained by 0.3mm slice width. A few features were disregarded in this model: (a) nostril hairs, (b) external nose shape, and (c) properties of nasal tissues such as, moist and warm condition within the nasal cavity. Only one of the two nasal cavities is studied considering that the anatomy of the nasal cavities is almost identical.

The data was then imported into software 3D-Slicer by The Slicer Community for volume rendering. It is a free source software and has been widely used particularly in medical purposes. Next, software 3Ds Max Design by Autodesk inc. was used to modify the 3D model of nasal cavity which includes deleting the unwanted features such as tongue, ethmoid sinuses, frontal sinus and many more. Feature variations that include smoothing process were also performed by using the same software. The modified model was imported to software ICEM CFD by ANSYS inc. by using STL data to generate the mesh consisting of prism elements near the wall and tetra elements in the other region before the airflow pattern is simulated by FLUENT 14.5 by ANSYS inc.

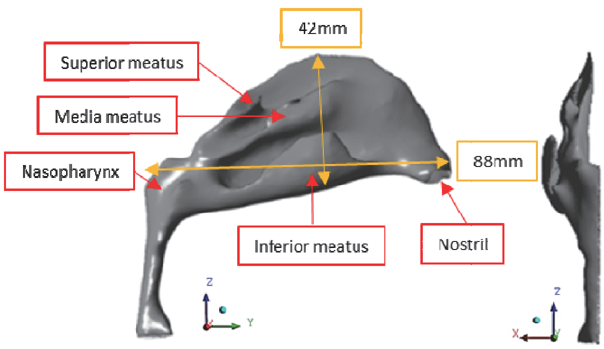

(a) Side view (left) and front view (right)

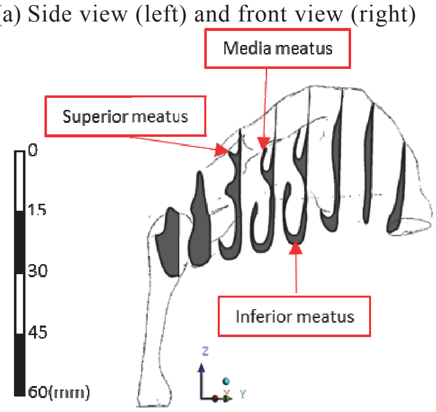

(b) Cross sectional area

Fig. 1 Anatomically realistic model of human nasal cavity

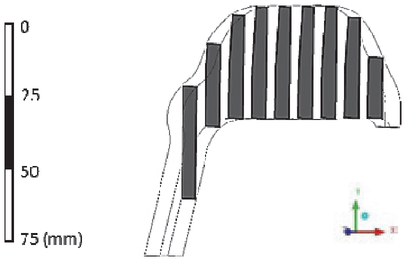

(a) Model A

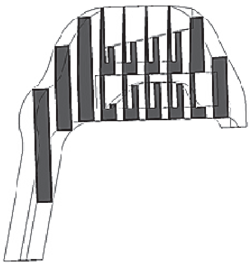

(b) Model B

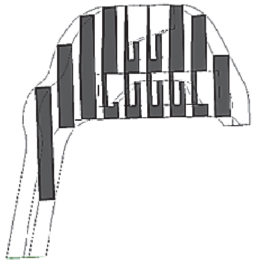

(c) Model C

(d) Model D

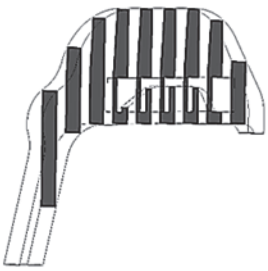

(e) Model E

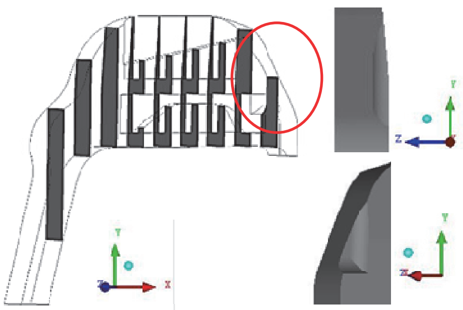

(f) Model F

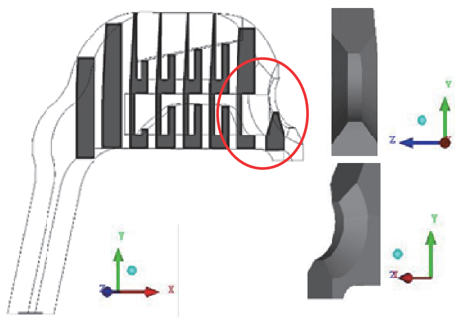

(g) Model G

Fig.2 Newly developed 3D simplified models

Table 3: General features of simplified models

Mod-el	Features	Media concha length (mm)	Inferior concha length (mm)
A	Without conchae	-	-
B	Long-media concha	48	48
C	Short-media concha	29	48
D	Media concha only	48	-
E	Inferior concha only	-	48
F	Model B+nasal valve a	48	48
G	Model B+nasal valve b	48	48

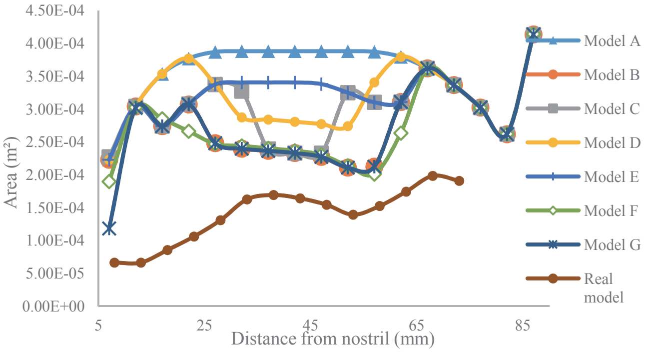

Fig. 3 Distribution of cross-sectional area (CSA) along models of nasal cavity. Location denotes the distance measured from the nasal vestibule.

2.1.2 *Variation of Simplified models*

Same as Part I for experimental study[13], 3D simplified models were generated on the basis of the elementary measurement of the real model such as maximum height, length and width, and the hydraulic diameter of inlet and outlet. Model generation method is similar to the real model, where, instead of CT scan data and 3D-Slicer, ANSYS Workbench was adopted. The conventional 3D simplified models[13] consist of common meatus and 3D turbinates inside pseudo 2D cavity model. Superior concha is ignored as it is assumed to be insignificant to the airflow patterns. Curves and bends are added to turbinates to resemble the real model. Further in the present research, an inclination angle is added to the superior region to present a narrow passageway in the upper side of the common meatus. Seven models (Model A ~ Model G) were designed as shown in Fig. 2 with feature variation given in Table 3.

Model B is accustomed to be the standard model and the following effects on the airflow pattern were studied:

(a) Without both conchae (Model A)
(b) Difference of length of media concha (Model B and C)
(c) The presence of either the media or inferior turbinates. Only one turbinate was investigated in each model (Model D and E)
(d) Addition of nasal valve (Models F and G) to model B: In Model F (Fig. 2 (f)) the common meatus is made narrow near the nostril by a triangular constriction, whereas in Model G (Fig. 2 (g)) the nasal cavity is straightly dissected in small part near the nostril area.

Figure 3 illustrates the distribution of the cross sectional area (CSA) of both type of models, anatomically realistic and simplified models. Tendency of CSA curves are similar to typical one shown in ref.8. The locally minimal area in the realistic model and Models F and G, which is located at 5-15 mm from the nostril, denotes the nasal valve.

2.2 *Computational condition*

The details of the computational condition for both models are illustrated in Tables 1 and 2. Reynolds number 880 was obtained from the hydraulic diameter of nares of the model and typical resting breathing rate[14)]. The maximum velocity at the trachea side is determined by the continuity equation, and the calculated velocity shown in Table 2 is imposed there as boundary conditions. A pressure of zero (Gauge pressure) was presumed at the nostril. The nasal wall is assumed to be rigid with non-slip condition. Due to low womersley number 1.6, almost no notable discrepancy can be observed in the numerical results between maximum respiration (inspiration and expiration) in unsteady condition and steady condition. Therefore in the present study, Navier-Stokes equations were numerically solved by use of FLUENT to simulate steady-state condition of human respiration.

2.3 *Grid convergence*

In order to obtain more accurate results without dependency of mesh size, before moving onto the simulation, grid convergence was investigated where the mesh is refined until the solution for the specified variable is converged to values independent on mesh size in condition of inspiration.

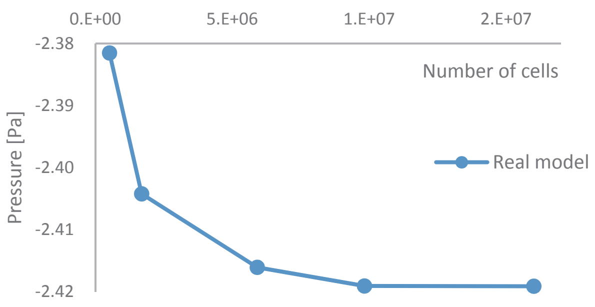

Fig. 4 Grid convergence in Real model in regards to pressure at local point near nasopharynx area

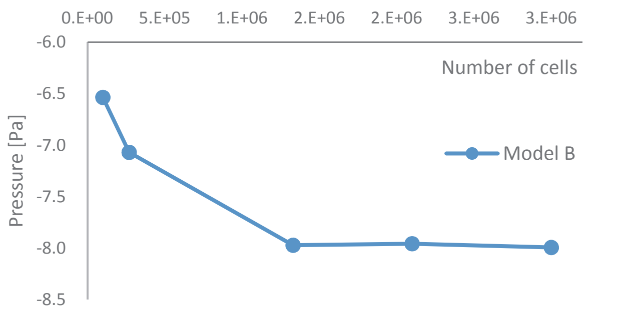

Fig. 5 Grid convergence in Simplified Model B in regards to pressure at local point nasopharynx area

Mesh consists of 5 layers of prism elements near the wall and tetra elements in the inner region was used in all models. In the realistic model, by changing the global element factor of ICEM CFD, in Model B, five types of grids with different mesh size were generated with 0.5 million cells being the coarsest and 16 million cells being the finest. For the steady solution of inspiration the pressure values at a point defined in the middle of the nasopharynx area are compared among all grids, since near the point the flow is complicated due to geometrical complexity. As shown in Fig. 4, the grid resolution was converged as the grid approached 9.8 million cells with less than 1% pressure difference with grid of 9.8 and 16 million cells. To save computing time and memory, the grid with 9.8 million cells was chosen to be the standard one for the realistic model throughout the present study.

As for simplified models in Fig. 5, the solution is considered converged as merely 1.5% discrepancy of pressure near the nasopharynx area can be observed between model with 1.33 million cells and 2.1 million cells as shown in Fig. 5. Therefore, model with 1.33 million cells was used through the entire study.

2.4 *Comparison of anatomically realistic model between computational and experimental results*

Numerical results of the realistic model are presented in distribution of streamlines and velocity magnitude during inspiration and expiration in Figs. 6 and 7, respectively.

The streamlines were derived from nostril and trachea area during inspiration and expiration, respectively. Meanwhile, in common and branch meatus, velocity and vectors were obtained from planes created in the particular area.

During inspiration in Fig. 6, a fairly large recirculation and small swirl are found near the olfactory region and nasopharynx area, respectively, the mainstream passes along the media region in the branch and common meatus. Meanwhile during expiration in Fig. 7, similar to inspiration results, small-scale swirls are observed at the opening of inferior meatus and nasopharynx area. High flow velocity distribution is recorded along media and inferior meatus. In the common meatus, flow magnitude in the media and inferior regions is higher compared to that in the superior region.

For comparison, experimental visualization[13)] is shown in Figs. 8 and 9 for inspiration and expiration, respectively. During inspiration, the similarities are found in the velocity distribution and the occurrence of swirls and also flow distribution in the common and branch meatus where the flow concentrated in media meatus. Meanwhile in the case of expiration, high velocity is noted in the middle and inferior meatus and swirls developed in the nasopharynx and inferior region in both results.

Overall, almost no significant difference can be observed in the airflow patterns between numerical and experimental results, and the reliability of numerical solutions has been confirmed on the airflow patterns.

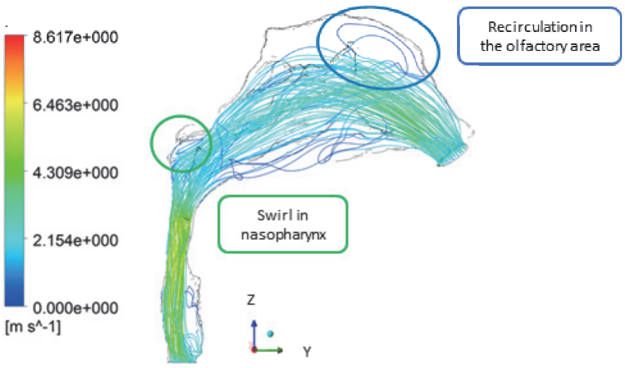

(a) Streamlines

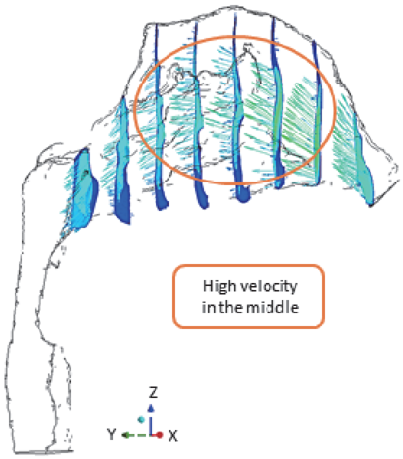

(b) Velocity distribution in magnitude and vectors in common meatus

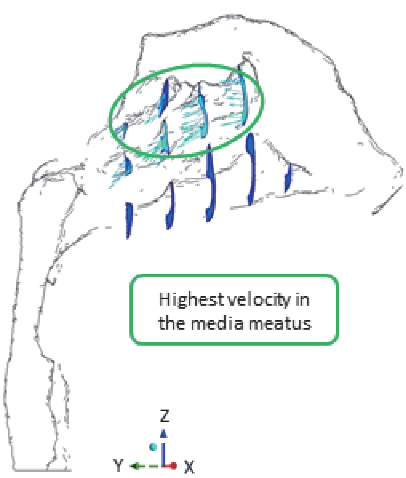

(c) Velocity distribution in magnitude and vectors in branch meatus

Fig. 6 Airflow pattern in real model during inspiration

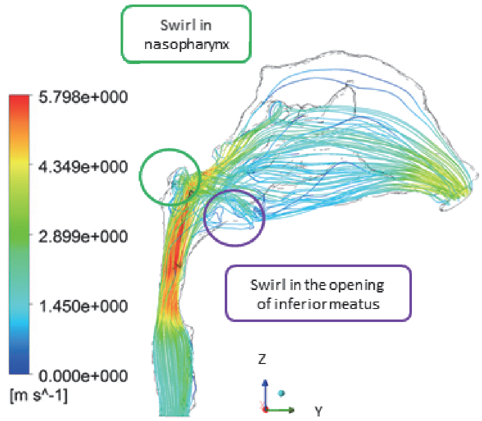

(a) Streamlines

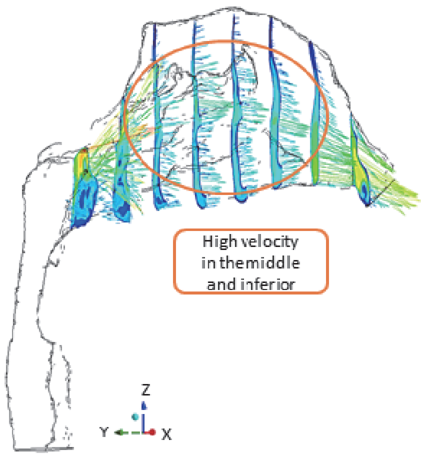

(b) Velocity distribution in magnitude and vectors in common meatus

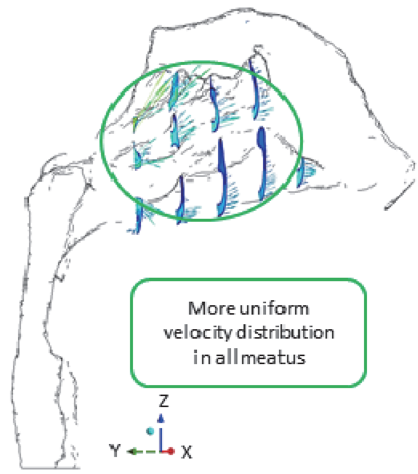

(c) Velocity distribution in magnitude and vectors in branch meatus

Fig. 7 Airflow pattern in real model during expiration

2.5 ***Modification of Simplified models***

The effects of the narrowed shape in the superior region of simplified models has been investigated, where the airflow patterns between the conventional model (without inclination at the walls of the pseudo 2D cavity) and modified model (with inclination in the superior region) are compared for analysis. As a typical case results of the standard model (Model B with long media concha) are presented here

Figures 10 (a) and (b) show comparison of the velocity- magnitude distributions and streamlines between conventional and modified models during inspiration and expiration, respectively. In general, discrepancy on the airflow patterns can be observed in the location of mainstream: the highest flow velocity is recorded along the media region in the modified model, while it is along the superior and media region in the conventional model.

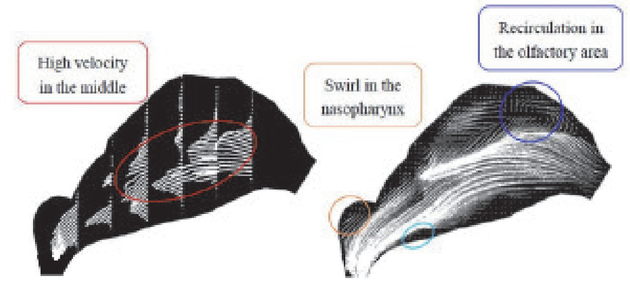

(a) Common meatus

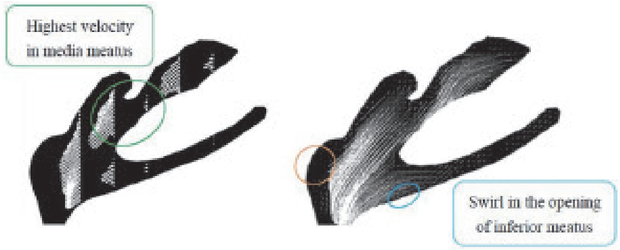

(b) Branch meatus

Fig.8 Pass lines during 0.06s and streamlines in inspiration[13)]

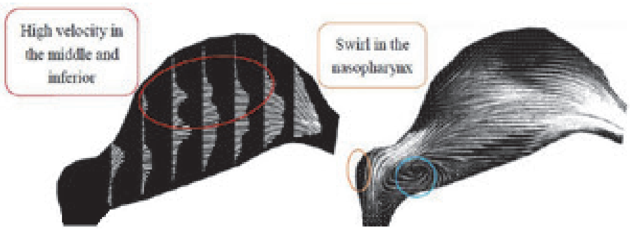

(a) Common meatus

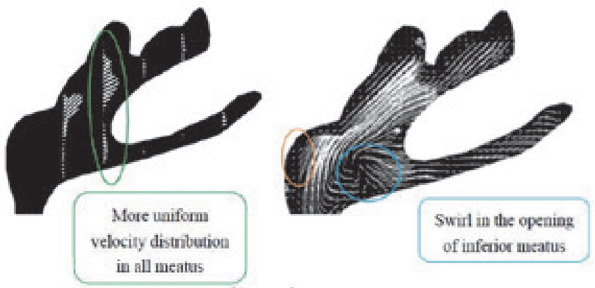

(b) Branch meatus

Fig.9 Pass lines during 0.06s and streamlines in expiration[13)]

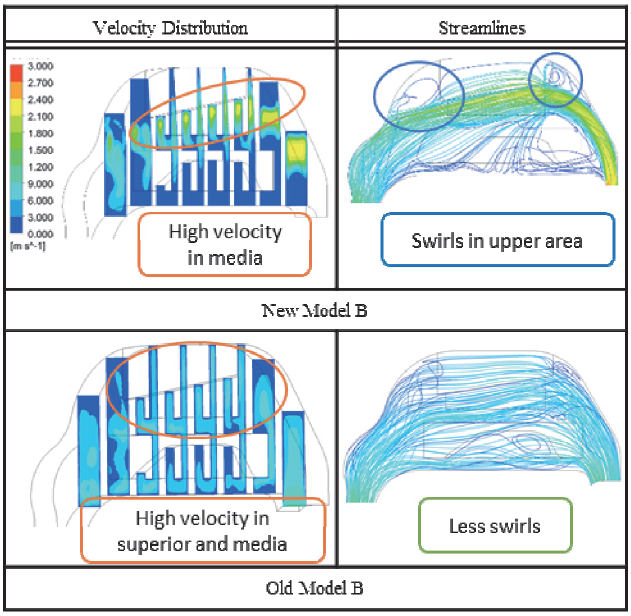

(a) Inspiration

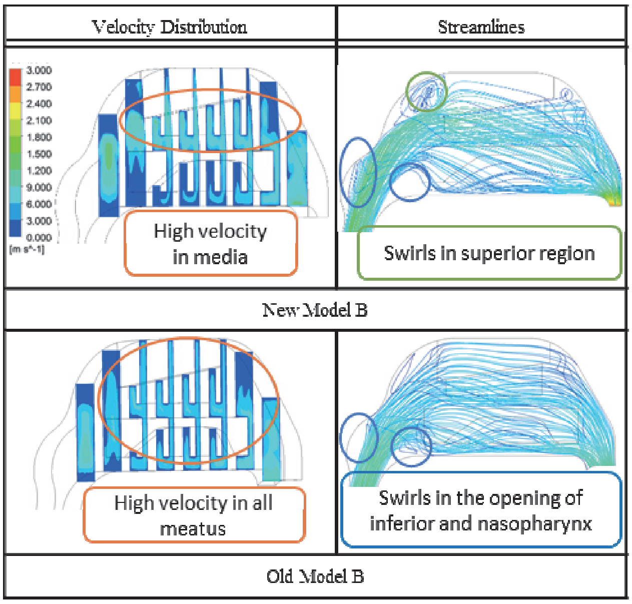

(a) Expiration

Fig. 10 Comparison of velocity distribution and streamlines

During inspiration, from the streamlines results, recirculation is detected in the upper anterior region in the modified model, which also can be seen near the olfactory area in the realistic model (Figs. 6 and 8(a)), but none in the conventional model. During expiration, in the modified model swirls occur in the nasopharynx area and at the opening of inferior meatus more clearly with swirl in the upper posterior region. These tendencies are observed also in the modified models other than Model B.

Thus it has been confirmed that the modified models yield flow patterns more similar to the realistic model than the conventional models.

3. Results and Discussion

Hereafter, results using the newly-modified models are shown.

3.1 *Mass flow rate*

As shown in Fig. 11, a plane which consists of cross sections for inferior, media and common meatus is defined at the mid-section of each simplified model B, C, F, G and the realistic model, in order to evaluate and compare the mass flow rate passing through the plane (Fig.12). Positive sign of mass flow rate represents the flow toward the throat.

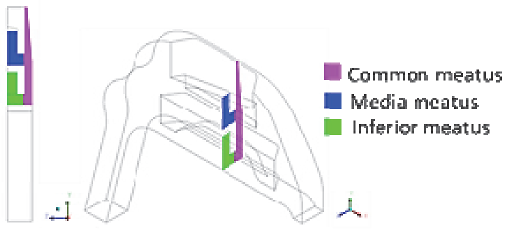

Fig. 11 Frontal view (left) and isometric view (right) of cross sectional plane for evaluation of mass flow rate

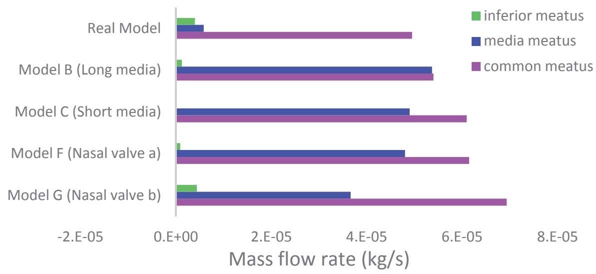

(a) Inspiration

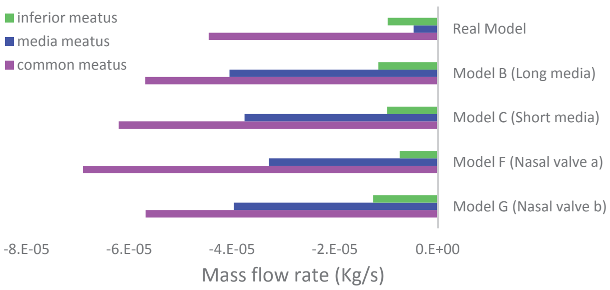

(b) Expiration

Fig. 12 Comparison of mass flow rate among Models B, C, F, and G and real model

3.1.1 *Inspiration*

In Fig. 12(a) during inspiration, Models B and C without nasal valves take negative values of the mass flow rate in the inferior meatus, which means that reversed flow occurs in the region. Between the two models, Model B with a longer media concha shows higher mass flow rate for the media meatus in comparison to Model C with a short media concha. On the other hand, Models F and G, with the presence of the nasal valve, take positive values of the mass flow rate in the inferior meatus, showing the similar pattern to the anatomically real model: the mass flow rate in common meatus is the highest and that in inferior meatus is the lowest. Between the two models, Model G shows better correspondence with the real model in the pattern that the mass flow rate in media and inferior meatus is significantly lower in comparison to that in the common meatus. In simplified models other than Model G, however, difference of the mass flow rate between media and common meatus is noticeably smaller.

3.1.2 *Expiration*

In the case of expiration in Fig. 12(b), the highest mass flow rate is recorded in the common meatus in all models. All simplified models take the second highest mass flow rate in the media meatus, but otherwise in the anatomically realistic model. This discrepancy might come from the wideness of the media meatus in the simplified models compared to the realistic model.

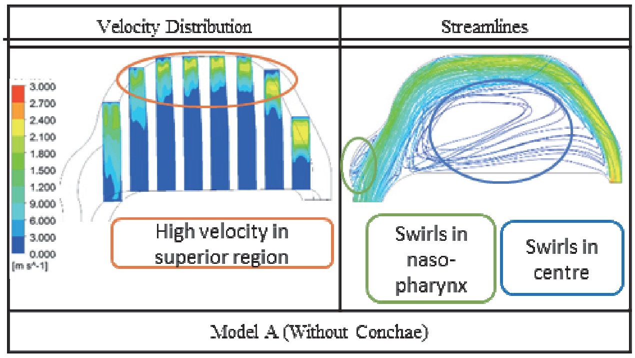

(a) Inspiration

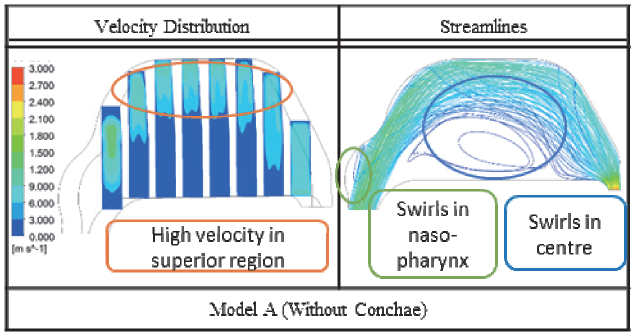

(b) Expiration

Fig. 13 Comparison of velocity distribution (left) and streamlines (right) in Model A

3.2 *Simplified Models (Without both conchae)*

3.2.1 *Inspiration*

In Fig. 13(a) during inspiration in Model A without both conchae, the mainstream fluid is conveyed through the superior region of the nasal cavity between the nostril and nasopharynx, guided by shape of the nasal cavity. A large-scale whirl is generated in the centre where the conchae should be located. A small swirl is generated near the opening nasopharynx area as a result of brief change in the geometry at the posterior airway passage

3.2.2 *Expiration*

Due to the geometry, the airflow is deflected at the opening nasopharynx and bypassed a small region in the upper side of the model during exhaling. From the streamlines in Fig 13(b), similar to the inspiration result, a large whirl is formed in the centre of the cavity and a small swirl develops at the posterior side near the nasopharynx area.

3.3 *Simplified Models (different length of media concha and existence of nasal valve)*

Figures 14 and 15 show the velocity-magnitude distribution and streamlines during inspiration and expiration, respectively, for simplified models with different length of media concha (Models B and C) and with the presence of nasal valve to Model B (Model F and Model G).

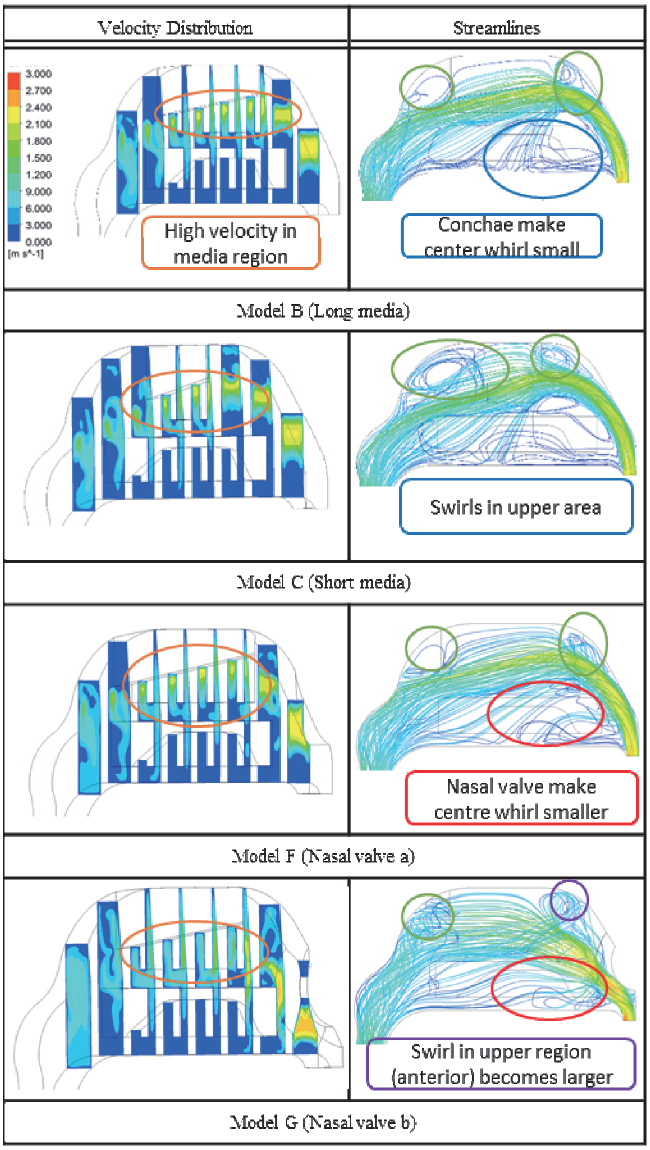

Fig. 14 Velocity distribution (left) and streamlines (right) in Models B, C and F during inspiration

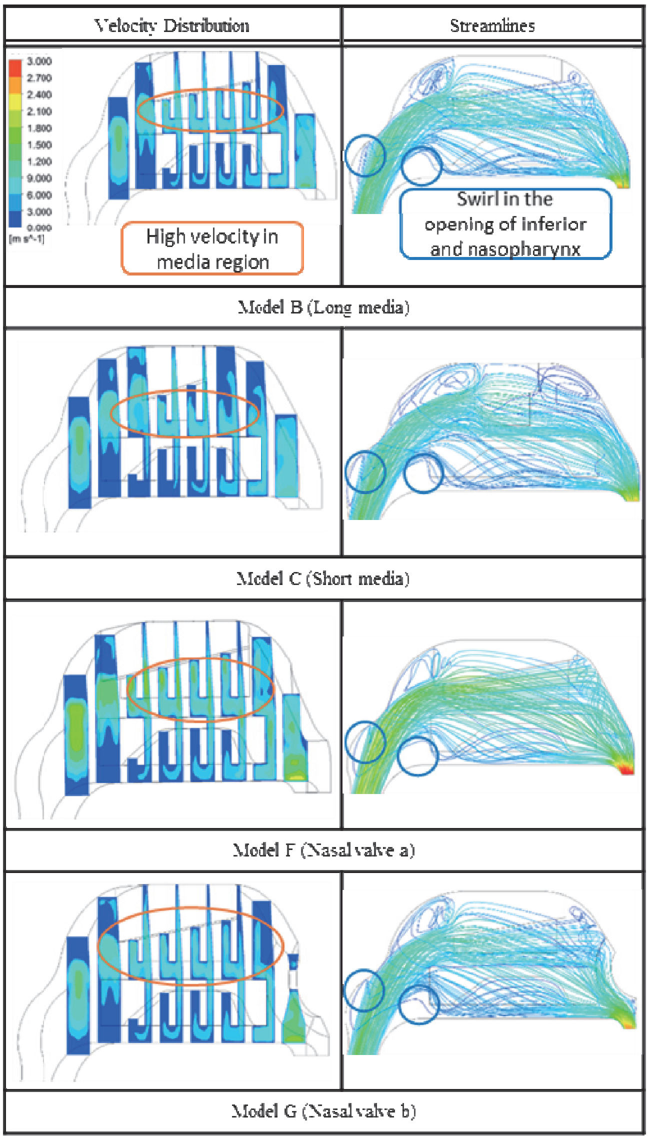

Fig. 15 Velocity distribution (left) and streamlines (right) in Models B, C and F during expiration

3.3.1 *Inspiration*

In Fig. 14 overall in velocity distribution, almost no significant difference in the flow velocity distribution can be observed, where high flow rate is recorded along the middle and common meatus in all models.

Regarding the length of the media concha, although the mass flow rate in the media meatus in Model B with a long media concha is higher than that in Model C with a short media concha (Fig 12(a)), no noticeable difference can be observed in the airflow pattern between both models. In the streamlines results for both models, small swirls are formed near the anterior and posterior sides in the superior region, and further the large-scale centre whirl observed in Model A (Fig. 13(a)) is made smaller but still exists: the flow reverts back to the nostril area as it passes through the inferior meatus (Fig. 12(a)). It is understood that the conchae make the centre whirl small. Although the same tendency can also be seen in Model F with a nasal valve, more flow goes forward to the nasopharynx area.

Overall, existence of the nasal valve in Models F and G helps to suppress the reversed flow in the inferior meatus. In Model G, with a varied nasal valve, the recirculation in the upper anterior region becomes larger in comparison to the other simplified models with conchae (Models B, C and F), which also can be seen near the olfactory area in the real model (Figs. 6 and 8(a)). It is understood that the nasal valve can increase the recirculated flow near the olfactory area.

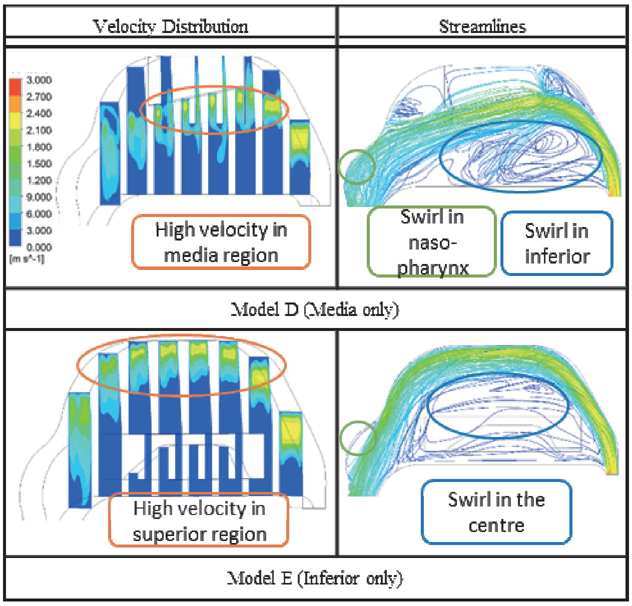

(a) Inspiration

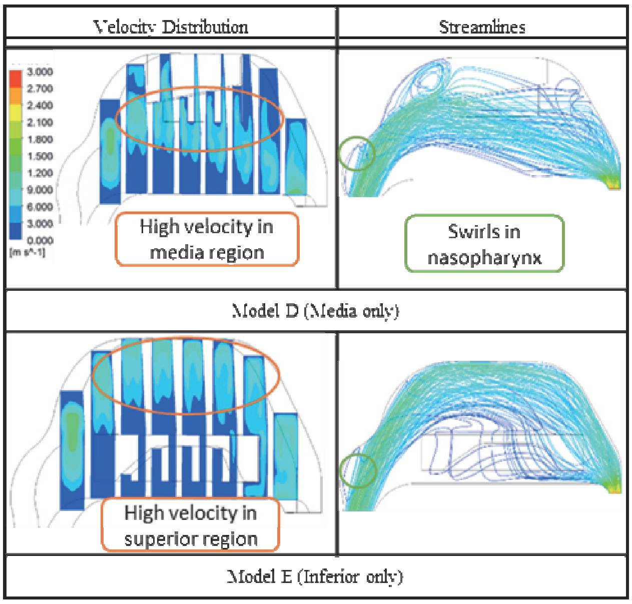

(b) Expiration

Fig. 16 Comparison of velocity distribution (left) and streamlines (right) between Models D and E

3.3.2 *Expiration*

In all models with conchae during exhaling, as shown in Fig. 15, generally, the airflow distributes more uniformly along the cavity in common meatus, medium-scale swirls are generated near the nasopharynx area and at the opening of inferior region, and the average velocity magnitude in the media meatus is larger compared to that in the inferior meatus. These tendencies also appear in the anatomically realistic model (Fig. 7 and Fig. 9).

Regarding the length of the media concha, although no noticeable difference can be observed in airflow patterns between Models B and C, the longer concha makes the mass flow rate in the media meatus higher (Fig. 12(b)), which is same as in inspiration results.

Furthermore, it is observed that the flow is introduced from the common meatus into the middle of inferior meatus.

3.4 *Simplified Models (Existence of media or inferior concha only)*

Figures 16 (a) and (b) show the velocity-magnitude distribution and streamlines during inspiration and expiration, respectively, for simplified models with existence of a long media concha only (Model D) and an inferior concha only (Model E).

3.4.1 *Inspiration*

From Fig. 16(a), without the inferior concha (Model D), almost no significant difference can be observed in the flow pattern in comparison to Model B, C, F and G, in the viewpoint that high flow velocity are recorded along the media region and swirls occur in the superior region. However, small swirls are generated in the area where the inferior concha should be located. As for Model E, the airflow tends to flow in the upper region along with the occurrence of swirls in the middle of the cavity, where the media concha should be located. In both models, small-scale swirls are detected at the nasopharynx area.

3.4.2 *Expiration*

During expiration shown in Fig. 16(b), similar to models with both conchae (Model B, C, F and G), Model D yields flow magnitude larger in the media region despite the non-existence of the inferior meatus, together with formation of small swirls near the entrance and exit of the media meatus in the superior region. Meanwhile, in Model E with the presence of inferior concha only, the mainstream tends to pass along the superior region, omitting half of the area in the posterior side of media meatus.

Thus the role of each concha is understood that the long media concha guides the flow into the media meatus, and the inferior concha prevents swirls from generating in the inferior region.

4. Discussion

In this study, improvements of simplified models have been imposed on the conventional models adopted in the experimental study (part Ⅰ) [13], by adding an inclination angle to the superior region to express the narrow passageway in the upper common meatus. As the comparison between simulation results and experimental results, similar to the anatomically realistic model, the mainstream of the airflow comes to passing along the media region, while in the conventional models the airflow tends to flow along the media and superior region.

The numerical study enables us to produce more information that is inaccessible by experimental methods such as the mass flow rate and detailed flow patterns. Furthermore, patching of nasal parts can be easily performed by use of simplified models. Therefore in the present study, by using the modified models with simplification, numerical simulation has been carried out to deduce and clarify the roles and functions of each nasal part as below.

4.1 *Inspiration*

The absence of both conchae causes a large-scale whirl in the centre of Model A. The presence of conchae makes the centre whirl small as observed in results of Model B, C, F and G. This result suggests that the conchae play a role as guide plates to reduce the size of the swirl, depending on the shape of nasal cavity, valve and conchae.

The centre whirl causes back flows in the inferior meatus. From viewpoint of the mass flow rate, in models without nasal valves (Models B and C) negative values in the inferior meatus indicate occurrence of reversed flows. The presence of a nasal valve, above all, Model G makes the distribution of mass flow rate almost similar to that in the anatomically realistic model, where the reversed flows are restricted in the inferior meatus.

As for the effect of media concha length, the longer media concha (Model B) makes the flow pass through the media meatus more. The reason why the longer media concha guides the flows into the media meatus is considered that the passage way abruptly becomes narrow between upper side of the nasal cavity and the end of media concha and therefore the flow along the superior region tends to stop.

The effect of each concha has been investigated by comparing flow patterns between the standard model and the model with the aimed concha only. Model D without an inferior concha shows the flow patterns almost similar to Models B, C, F and G in the media and superior region. However, small swirls are generated where the inferior concha should be located. As for Model E without a media concha, the fluid tends to flow in the upper region along with the occurrence of swirls in the middle of the cavity where the media concha should be located.

From the above comparisons the role of each concha is deduced: the long media concha makes the flow pass along media region. Both media and inferior conchae are needed to guide the flow more uniformly with repression of swirl formation.

In general, Model G exhibits the most similar airflow pattern to the real model in the following points: mainstream is located in the media region with restrained reversion of flow in the inferior meatus; and large recirculation is generated in the upper anterior region corresponding to the olfactory area.

4.2 *Expiration*

With regard to the distribution of mass flow rate, much difference is not observed among simplified models, although there appears slightly the similar tendency as the inspiration results that the longer media concha guides more flow into the media meatus. The ratio of mass flow rate passing the common meatus is highest and dominant in both the anatomically realistic and simplified models, leading to the uniform distribution of airflow along the cavity in the common meatus in expiration. In the ratio of mass flow rate passing the middle meatus there is large discrepancy between the realistic model and simplified models, which would be due to the wider media meatus in the simplified models. This suggests geometrical improvements of simplified models so that the ratio of representative area for the common, media, and inferior meatus could agree with that of the realistic models.

In Model A, similar to inspiration results, without both conchae a large-scale whirl occurs in the middle of the cavity. The similarity between the real model and all simplified models is found in the occurrence of small swirls in the upper side of the nasopharynx area and at the opening of inferior meatus, which comes from the similarity of shape in the corresponding part. With absence of either inferior or media concha in Model D or E, the fluid tends to flow also in the area where the concha should be located.

From the above, it is deduced that the role of conchae during expiration is to guide the flow into the media meatus with the curved shape of nasopharynx, and to make the flow in the common meatus distribute evenly.

5. Conclusion

In this numerical study, regarding flows within nasal cavities, first, numerical solutions have been successfully validated by comparison with experimental visualization on the anatomically realistic model of the nasal cavity with a complicated configuration and the conventional simplified models.

Modelling study has been carried out to clarify rolls and functions on human nasal morphology. As a result, it has been confirmed that Model G (with longer media concha and varied nasal valve) is the most similar to the realistic model in flow patterns including distributions of mass flow rate. The roles of each nasal portion have been made clear as follows:

1) By narrowing the upper side of the cavity, the flow tends to pass along the media meatus which can also be found in the real mode, instead of middle and superior region.

2) The two conchae, in one united body, play a role as guide plates to distribute the flow more uniformly with restriction of swirl formations;

3) The role of the media concha is to determine the airflow distribution in three meatus: the longer media concha makes the flow pass the media meatus;

4) The nasal valve plays a role in the occurrence of recirculation in the olfactory region and also to reduce reversed flow in the inferior meatus during inspiration.

Thus, complicated flow phenomena within the realistic model have been comprehended with the help of simplified models.

However, there remain problems on modelling of simplified nasal geometries such as ratio of areas for common, media and inferior meatus, which might cause disagreement of ratio of flow rate for common and branch meatus between the realistic and simplified models. In the near future modeling study is needed, including variation of the anatomically realistic model.

Reference

1) Bachmann W, Legler U. Studies on the structure and function of the anterior section of the nose by means of luminal impressions. *Acta Otolaryngol*. 73:433-42. 1972

2) Carlos E, Nazareth N, Josiane F, Olavo M, Jodo F. Nasal Valve: anatomy and physiology. *Brazilian journal of Otorhinolaryngology* 75(2). 2009

3) E. Afiza, Y. Kurashina, Y. Takakura, T. Atsumi, and M. Iida, Investigation of Airflow Patterns within Real and Simplified Models of Nasal Cavities, *The 12th International Symposium on Fluid Control, Measurement and Visualization, FLUCOME*, 2013.

4) C.E. Rennie, C.M. Hood, E.J.S.M. Blenke, R.S. Schroter, D.J. Doory, et al., Physical and Computational Modeling of Ventilation of the Maxillary Sinus, *Head and Neck Surgery*, pp.164-170, 2011.

5) Y. Izumi, T.Tajikawa, K.Ohba, Y. Uesugi, In vitro experiment on reciprocating flow in a model of the nasal cavities and pharynx, *The Proceedings of the 19th Bioengineering Conference*, *The Japan Society of Mechanical Engineers,* 2007.

6) Hopkins LM, Kelly JT, Prasad AK, and Wexter AS, Particle image velocimetry measurements in complex geometries. *Exp Fluids 29:91-95, 200. (11)*

7) Doorly, D.J., Taylor, D.J., Gambarutto, A.M., Schroter, R.C., Tolley, N., 2008b. Nasal architecture: form and flow. Philos. Trans. R. Soc. A 366, 3255-3246, dio:10.1098/rsta.2008.0083 (12)

8) D.J. Doorly, D.J. Taylor, and R.C. Schroter, Mechanics of Airflow in the Human Nasal Airways, *Respiratory Phsyiology &Neurobiology*, Vol. 163, pp.100-110, 2008 (13)

9) T. Sakata, G. Tanaka, T. Sera, N. Kakusho, H. Yokota, K. Ono, and S. Takagi, Voxel Simulation of Nasal Cavity, *The Proceedings of 22nd Bioengineering Conference*, *The Japan Society of Mechanical Engineers,* 2010. (14)

10) Keyhani, K., Scherer, P.W., Mozell, M.M. Numerical Simulation of airflow in the human nasal cavity. J. Biomech. Eng. 117, 429-441. 1995

11) E.Afiza, Y.Takakura, Y. Takakura, T. Atsumi, M. Iida, On Airflow Patterns within Real and simplified models of nasal cavities (Comparison of numerical simulation with experiments). *Proceedings of the 26th Bioengineering Conference*, *The Japan Society of Mechanical Engineers,* 2014.

12) E. Alias, A. Ariffin, Y. Takakura, T. Atsumi, M.Iida, Investigation of Airflow Patterns within Real and Simplified Models of Nasal cavities (Variation of Simplified models), *16th International Symposium on Flow Visualization, June 24-28*, Okinawa, 2014

13) E. Alias, Y. Takakura, T. Atsumi, M.Iida, Airflow pattern within Real and 3D simplified Models of Nasal Cavities (Ⅰ . Experimental Study), Proc. Schl. Tokai University (to appear).

14) Y. Izumi, T.Tajikawa, K.Ohba, Y. Uesugi, In vitro experiment on reciprocating flow in a model of the nasal cavities and pharynx, *The Proceedings of the 19th Bioengineering Conference*, *The Japan Society of Mechanical Engineers,* 2007.